EARTHQUAKE ENGINEERING AND STRUCTURAL DYNAMICS, VOL. 25, 333–355 (1996)

EVALUATION OF SOME IMPLICIT TIME-STEPPING ALGORITHMS FOR PSEUDODYNAMIC TESTS

ORESTE S. BURSI

Department of Structural Mechanics and Design Automation, University of Trento, Via Mesiano 77, 38050 Trento, Italy

AND

PUI-SHUM B. SHING

Department of Civil, Environmental and Architectural Engineering, University of Colorado, Boulder, CO 80309-0428, U.S.A.

SUMMARY

Two types of implicit time-stepping algorithms have been proposed recently for pseudodynamic tests. The first type consists of an algorithm which relies on Newton iterations to satisfy the equations of motion. The second type consists of an algorithm which is based on the *Operator-Splitting* technique and does not require any numerical iteration. While one or the other has been preferred by some researchers, these time-stepping algorithms have not been analysed and compared under a uniform setting. In this paper, a concise summary of these schemes is presented, and they are evaluated in a consistent manner in terms of numerical dissipation, frequency distortion and experimental errors. The analytical results are validated by numerical simulations as well as experimental results. It is shown that the algorithm based on Newton iterations can control experimental error effects effectively by means of an error-correction procedure. The algorithm based on the *Operator-Splitting* technique demonstrates similar performance provided the *I-Modification* is adopted.

KEY WORDS: pseudodynamic tests; non-linear response; implicit time-stepping algorithms; numerical errors; experimental errors; seismic performance

INTRODUCTION

The pseudodynamic method is an on-line computer controlled test technique for evaluating the seismic performance of structures. For testing stiff multiple-degree-of-freedom structures and substructures, several implicit time-stepping algorithms have been recently developed.[1–3] They are all special adaptations of the α-method proposed by Hilber *et al.*[4]

Thewalt and Mahin[1] have developed the first successful implicit scheme for testing inelastic multiple-degree-of-freedom structures based on a hybrid digital-analog approach. This time-stepping scheme, which is based on the α-method developed by Hilber *et al.*,[4] has proved to be reliable and far superior to explicit schemes.

For testing structural subassemblies, which often have high-frequency components introduced by the interface degrees of freedom, Nakashima *et al.*[2] have successfully implemented an unconditionally stable algorithm, termed the *Operator-Splitting* algorithm, based on a technique originally proposed by Hughes *et al.*[5] This scheme relies on a predictor–corrector approach and does not require any numerical iteration. It has been used recently by Tsai *et al.*[6] for testing structural subassemblies.

A third scheme has been developed by Shing *et al.*[3] for testing general multiple-degree-of-freedom structures. This implicit algorithm is based on the α-method of Hilber *et al.*[4] and relies on a modified Newton-type iterative procedure. Later, an adaptive time-stepping procedure has been introduced into this scheme for testing structural models which may exhibit severe strain softening.[7] Recent applications of this algorithm include the pseudodynamic testing of a stiff full-scale, multiple-storey, masonry structure[8] and a subassembly of a steel braced frame.[9] The latter is based on substructuring techniques.

CCC 0098–8847/96/040333–23

Received 19 November 1994
Revised 16 October 1995

It is evident that the reliability of a pseudodynamic test depends on the accuracy of the time-stepping scheme used. In addition, different studies have shown that the pseudodynamic test method is very sensitive to experimental errors.[10,11] The error-propagation characteristics of the hybrid method of Thewalt and Mahin[1] have been analysed by Peek and Yi[12,13] and Shing and Vannan.[14] Since the algorithmic and error-propagation properties of this scheme are identical to those of the α-method, it will not be considered further here.

The error-propagation characteristic of the *Operator-Splitting* scheme have been studied by Nakashima and Kato[11] and Comberscure and Pegon.[15] Finally, the error-propagation characteristics of the iterative-based scheme of Shing *et al.*[3] have been thoroughly investigated by Shing *et al.*[3] and Comberscure and Pegon.[15]

As results of these studies, different error-compensation techniques[3,11,16-18] have been developed. In particular, Nakashima and Kato[11] have proposed an error-compensation technique called the *I-Modification*, which is based on the predictor stiffness of a structure and the difference between the commanded and measured displacements. Recently, Nakashima *et al.*[16] have proposed that experimental error growth be controlled by the dissipative properties of the α-method.[4] To reduce the effect of experimental errors, Shing *et al.*[3] have introduced a correction procedure for residual errors. It has been shown that this procedure can eliminate effectively the spurious higher-mode response of a structure.[17]

In spite of various studies and applications, the aforementioned algorithms have not been evaluated in a consistent and uniform manner, and their pros and cons are not well understood. The main purpose of the study presented in this paper is to compare these algorithms in a uniform setting in terms of numerical and experimental error effects. The analytical results are substantiated with numerical simulations and experimental results.

IMPLICIT TIME-STEPPING ALGORITHMS FOR NON-LINEAR PROBLEMS

Two types of implicit time-stepping algorithms developed for pseudodynamic tests are considered in the following sections. The first is an algorithm based on the modified Newton iteration, which has been developed by Shing *et al.*[3] and is denoted as the α–*C* algorithm in this paper. The second type is a time-stepping method based on the *Operator-Splitting* technique, which does not require any numerical iteration. This is referred to as the α–OS algorithm and was proposed by Nakashima *et al.*[11,16] for pseudodynamic tests. A concise summary of these time-stepping algorithms is presented in the following sections. They are all special adaptations of the α-method proposed by Hilber *et al.*[4]

α–C algorithm

The α–*C* algorithm is essentially the α-method[4] endowed with the modified Newton iteration and an error-correction procedure proposed by Shing *et al.*[3] The α-method adopts the following modified equations of motion:

$$\mathbf{M}\mathbf{a}_{i+1} + (1+\alpha)\mathbf{C}\mathbf{v}_{i+1} - \alpha\mathbf{C}\mathbf{v}_i + (1+\alpha)\mathbf{r}_{i+1} - \alpha\mathbf{r}_i = (1+\alpha)\,\mathbf{f}_{i+1} - \alpha\mathbf{f}_i \tag{1}$$

in which $\mathbf{M}$ and $\mathbf{C}$ are the mass and damping matrices of a structure, $\mathbf{v}_i$ and $\mathbf{a}_i$ are vectors of nodal velocities and accelerations at time equal to $i\Delta t$, where Δt is the integration time step, $\mathbf{r}_i$ is the nodal restoring force vector and $\mathbf{f}_i$ is the external force excitation. In this method, the nodal displacements, $\mathbf{d}_{i+1}$, and nodal velocities, $\mathbf{v}_{i+1}$, are approximated by the following difference equations:

$$\mathbf{d}_{i+1} = \tilde{\mathbf{d}}_{i+1} + \Delta t^2\beta\mathbf{a}_{i+1} \tag{2}$$

$$\mathbf{v}_{i+1} = \mathbf{v}_i + \Delta t[(1-\gamma)\mathbf{a}_i + \gamma\mathbf{a}_{i+1}] \tag{3}$$

where

$$\tilde{\mathbf{d}}_{i+1} = \mathbf{d}_i + \Delta t\mathbf{v}_i + \Delta t^2[(\tfrac{1}{2}-\beta)\mathbf{a}_i] \tag{4}$$

and α, β and γ are parameters that govern the numerical properties of this algorithm. When $\alpha \in [-\frac{1}{3}, 0]$, $\gamma = (1 - 2\alpha)/2$ and $\beta = (1 - \alpha)^2/4$, this time-stepping method is unconditionally stable and attains a second-order accuracy.[4] It also has favourable energy-dissipation properties.

To evaluate the response of a non-linear system for given initial conditions and a discretized excitation function $\mathbf{f}_i$, the α–C algorithm can be implemented as follows.

Predictor phase:

$$\mathbf{d}_{i+1}^{(0)} = \mathbf{d}_i \tag{5}$$

$$\mathbf{r}_{i+1}^{(0)} = \mathbf{r}_i \tag{6}$$

Multi-corrector phase: Solve

$$\mathbf{K}^* \Delta \mathbf{d}_{i+1}^{(k)} = \mathbf{R}_{i+1}^{(k)} \tag{7}$$

for $\Delta \mathbf{d}_{i+1}^{(k)}$, where

$$\mathbf{K}^* = \bar{\mathbf{K}} + (1 + \alpha)\mathbf{K} \tag{8}$$

$$\bar{\mathbf{K}} = \frac{1}{\Delta t^2 \beta} \mathbf{M} + \frac{(1 + \alpha)\gamma}{\Delta t \beta} \mathbf{C} \tag{9}$$

$$\begin{aligned} \mathbf{R}_{i+1}^{(k)} = & -\bar{\mathbf{K}} \mathbf{d}_{i+1}^{(k)} - (1 + \alpha)\mathbf{r}_{i+1}^{(k)} + \bar{\mathbf{K}} \tilde{\mathbf{d}}_{i+1} \\ & + (1 + \alpha)\mathbf{f}_{i+1} - \alpha \mathbf{f}_i - \mathbf{C}\mathbf{v}_i - (1 + \alpha)(1 - \gamma)\Delta t \mathbf{C}\mathbf{a}_i + \alpha \mathbf{r}_i \end{aligned} \tag{10}$$

Correct the displacements and restoring forces in the following manner:

$$\mathbf{d}_{i+1}^{(k+1)} = \mathbf{d}_{i+1}^{(k)} + \Delta \mathbf{d}_{i+1}^{(k)} \tag{11}$$

$$\mathbf{r}_{i+1}^{(k+1)} = \mathbf{r}(\mathbf{d}_{i+1}^{(k+1)}) \tag{12}$$

Updating phase: After convergence,

$$\mathbf{d}_{i+1} = \mathbf{d}_{i+1}^{(l)} + \Delta \mathbf{d}_{i+1}^{(l)} \tag{13}$$

$$\mathbf{r}_{i+1} = \mathbf{r}_{i+1}^{(l)} + \mathbf{K} \Delta \mathbf{d}_{i+1}^{(l)} \tag{14}$$

$$\mathbf{a}_{i+1} = \frac{1}{\Delta t^2 \beta} (\mathbf{d}_{i+1} - \tilde{\mathbf{d}}_{i+1}) \tag{15}$$

$$\mathbf{v}_{i+1} = \mathbf{v}_i + \Delta t[(1 - \gamma)\mathbf{a}_i + \gamma \mathbf{a}_{i+1}] \tag{16}$$

in which $\Delta \mathbf{d}_{i+1}^{(l)}$ represents a residual displacement vector which satisfies the convergence criteria that $|\Delta d_{i+1}^{(l)}| \leqslant \Delta d^n$, where Δd^n is a preset displacement tolerance for each degree-of-freedom n.[3] To obtain accurate results, Shing *et al.*[3] have recommended a convergence tolerance that can be as large as 6 per cent of the expected maximum displacement for linearly elastic structures, and 2 per cent for inelastic structures with strain hardening. For structures with severe strain softening, a convergence tolerance of 0·2 per cent has been suggested by Bursi and Shing.[20]

In this scheme, $\mathbf{K}$ represents a predictor stiffness matrix, $\mathbf{R}_{i+1}^{(k)}$ a residual error vector and k is an iteration index. To apply the above algorithm, it is necessary that the predictor stiffness $\mathbf{K}$ used in the iteration be higher than or equal to the actual stiffness $\mathbf{K}^a$ of a structure,[3] i.e. $\delta \mathbf{K} = \mathbf{K} - \mathbf{K}^a$ be positive semi-definite.

The error correction performed in equations (13) and (14) reduces the effect of stepwise residual errors on numerical results, and eliminates the spurious higher-mode response that could otherwise be excited by residual errors. The iteration and the error-correction procedure are illustrated in Figures 1(a) and 1(b), respectively, for a single-degree-of-freedom system, in which inertia and damping are ignored. This algorithm can be implemented with a dual displacement control, by using displacement transducers external as well as internal to hydraulic actuators. This prevents the deformation of the reaction frame supporting the actuators from affecting the actual structural displacements, while avoiding any external disturbance to the transducers

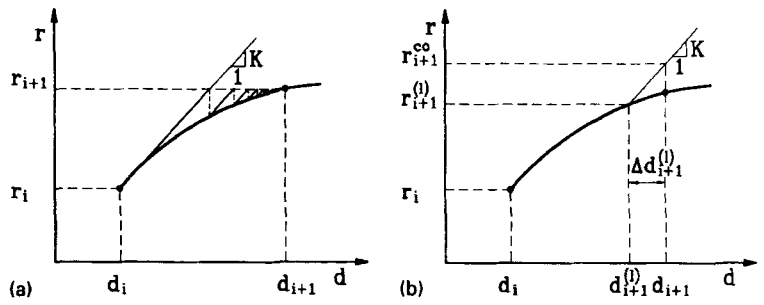

Figure 1. Non-linear solution method for the α–C algorithm: (a) modified Newton iterations; (b) correction for residual errors

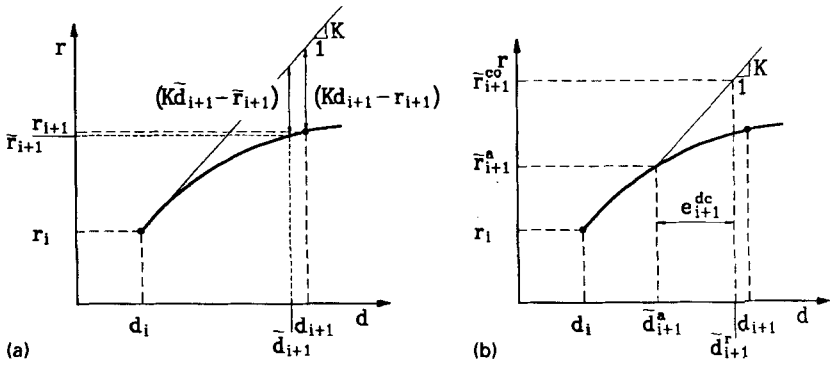

Figure 2. Solution method for OS algorithms: (a) correction for non-linearity; (b) *I-Modification* for displacement control errors

used in the servo-control loop. The implementation of this algorithm appears as easy as that of explicit schemes, and the multi-correction procedure allows residual errors introduced in each integration step to be controlled appropriately.[3]

α–OS algorithm

The α–OS algorithm is the synthesis of the *Operator-Splitting* technique[5] with the α-method.[4] This results in an explicit predictor-implicit corrector algorithm[16] with the following equations of motion:

$$\mathbf{M}\mathbf{a}_{i+1} + (1+\alpha)\mathbf{C}\mathbf{v}_{i+1} - \alpha\mathbf{C}\mathbf{v}_i + (1+\alpha)(\mathbf{K}\mathbf{d}_{i+1} + \tilde{\mathbf{r}}_{i+1} - \mathbf{K}\tilde{\mathbf{d}}_{i+1})$$
$$- \alpha(\mathbf{K}\mathbf{d}_i + \tilde{\mathbf{r}}_i - \mathbf{K}\tilde{\mathbf{d}}_i) = (1+\alpha)\mathbf{f}_{i+1} - \alpha\mathbf{f}_i \tag{17}$$

in which $\mathbf{d}_{i+1}$ and $\mathbf{v}_{i+1}$ are approximated by the formulas defined in equations (2)–(4). With the *Operator-Splitting* technique, the deviation of the structural response from linearity is approximated as

$$\mathbf{K}\mathbf{d}_{i+1} - \mathbf{r}_{i+1} \approx \mathbf{K}\tilde{\mathbf{d}}_{i+1} - \tilde{\mathbf{r}}_{i+1} \tag{18}$$

in which $\mathbf{K}$ represents a predictor stiffness matrix, $\tilde{\mathbf{d}}_{i+1}$ is determined with equation (4), and $\tilde{\mathbf{r}}_{i+1}$ is the restoring force vector developed by the structure when the predictor displacements $\tilde{\mathbf{d}}_{i+1}$ have been imposed. This approximation avoids any numerical iteration and is illustrated in Figure 2(a) for a single-degree-of-freedom system with zero inertia and damping.

A necessary condition for the unconditional stability of this algorithm is that $\delta\mathbf{K}_{i+1} = \mathbf{K} - \mathbf{K}_{i+1/2}$ must be positive semi-definite, where matrix $\mathbf{K}_{i+1/2}$ is the tangent stiffness at time step $(i + \frac{1}{2})\Delta t$.[21]

The α–OS algorithm can be implemented for pseudodynamic tests as follows.

Predictor phase: Evaluate a predictor displacement vector with equation (4).

Corrector phase: Solve

$$\mathbf{K}^*(\mathbf{d}_{i+1} - \tilde{\mathbf{d}}_{i+1}) = -(1+\alpha)\tilde{\mathbf{r}}_{i+1} + \bar{\mathbf{P}}_{i+1} \tag{19}$$

for $\mathbf{d}_{i+1}$, where

$$\tilde{\mathbf{r}}_{i+1} = \mathbf{r}(\tilde{\mathbf{d}}_{i+1}) \tag{20}$$

$$\bar{\mathbf{P}}_{i+1} = (1+\alpha)\mathbf{f}_{i+1} - \alpha\mathbf{f}_i - \mathbf{C}\mathbf{v}_i - (1+\alpha)(1-\gamma)\Delta t\mathbf{C}\mathbf{a}_i + \alpha(\mathbf{K}\mathbf{d}_i + \tilde{\mathbf{r}}_i - \mathbf{K}\tilde{\mathbf{d}}_i) \tag{21}$$

Updating phase:

$$\mathbf{a}_{i+1} = \frac{1}{\Delta t^2 \beta}(\mathbf{d}_{i+1} - \tilde{\mathbf{d}}_{i+1}) \tag{22}$$

$$\mathbf{v}_{i+1} = \mathbf{v}_i + \Delta t[(1-\gamma)\mathbf{a}_i + \gamma\mathbf{a}_{i+1}] \tag{23}$$

To mitigate the effects of displacement control errors in pseudodynamic tests, Nakashima and Kato[11] have introduced a correction technique, which they called the *I-Modification*. It simply corrects the restoring force vector as follows:

$$\tilde{\mathbf{r}}^{\mathrm{co}}_{i+1} = \tilde{\mathbf{r}}^{\mathrm{a}}_{i+1} - \mathbf{K}(\tilde{\mathbf{d}}^{\mathrm{a}}_{i+1} - \tilde{\mathbf{d}}^{\mathrm{r}}_{i+1}) \tag{24}$$

in which $\tilde{\mathbf{d}}^{\mathrm{r}}_{i+1}$ denotes the exact numerical solution, $\tilde{\mathbf{d}}^{\mathrm{a}}_{i+1}$ and $\tilde{\mathbf{r}}^{\mathrm{a}}_{i+1}$ represent experimental feedback quantities, and $\tilde{\mathbf{r}}^{\mathrm{co}}_{i+1}$ denotes the corrected restoring force vector. The *I-Modification* is illustrated in Figure 2(b) for a single-degree-of-freedom system in which inertia and damping are ignored.

From now on, the α–OS algorithm with the *I-Modification* is referred to as the α–OSM algorithm. The α–OSM algorithm offers the main benefit of simplicity in implementation and no numerical iteration. However, in such a scheme, each predictor–corrector step is equivalent to the first iteration of a modified Newton procedure. As a result, a degradation in accuracy is expected when the predictor stiffness is very different from the actual stiffness of a structure, or when the structural specimen exhibits a severe non-linearity. To reduce these effects, small integration time intervals as well as accurate displacement measurements and servo-controls have to be used.

COMPARISON OF IMPLICIT ALGORITHMS WITHOUT EXPERIMENTAL ERRORS

In this section, the α–C and α–OSM algorithms as analysed and compared with the experimental error effects ignored. Under these conditions, the α–C algorithm has the same dissipation and frequency distortion properties as the α-method.[4] However, with numerical convergence errors, additional energy effects will be introduced by the error corrections shown in equations (13) and (14), as has been investigated by Shing *et al.*[3] In the absence of experimental errors, the α–OSM algorithm is identical to the α–OS algorithm.

As mentioned in the previous section, to apply the α–C and α–OSM algorithms, it is necessary that the difference between the predictor and the actual stiffness of a structure, i.e. $\delta\mathbf{K} = \mathbf{K} - \mathbf{K}^{\mathrm{a}}$, be positive semi-definite. When $\delta\mathbf{K} = \mathbf{0}$, these algorithms degenerate to the α-method.[4] However, experimental evidence indicates that it is difficult to measure the actual stiffness of a structure in a very precise manner. Therefore, a discrepancy between the predictor stiffness and the actual stiffness of a structure is expected to be inevitable and it will affect the accuracy of these algorithms.

The stability and accuracy of the α–OS algorithm have been studied by Nakashima *et al.*[16] However, to compare the properties of the α–C and α–OSM algorithms in a consistent fashion, it appears advantageous to analyse the dissipation and frequency distortion properties of the α–OSM algorithm in the following manner.

For a linearly elastic single-degree-of-freedom system,[4] the algorithm can be expressed in the following one-step recursive form:

$$\mathbf{x}_{i+1} = \mathbf{A}\mathbf{x}_i + (1+\alpha)\mathbf{L}f_{i+1} - \alpha\mathbf{L}f_i \tag{25}$$

where the amplification matrix, **A**, and the load operator, **L**, are defined as

$$\mathbf{A} = \frac{1}{D}\begin{bmatrix} 1 + \{(1+\alpha)\beta(K/K^a)\Omega^2 - \beta\Omega^2\} & 1 + \{(1+\alpha)\beta(K/K^a)\Omega^2 - (1+\alpha)\beta\Omega^2\} & (\tfrac{1}{2}-\beta)(1+(1+\alpha)\beta(K/K^a)\Omega^2) + \{\alpha\beta^2\Omega^2 + \beta\Omega^2[\beta - \tfrac{1}{2}(1+\alpha)]\} \\ -\gamma\Omega^2 & 1 + \{(1+\alpha)\beta(K/K^a)\Omega^2 - (1+\alpha)\gamma\Omega^2\} & (1-\gamma)(1+(1+\alpha)\beta(K/K^a)\Omega^2) + \{\alpha\beta\gamma\Omega^2 + \gamma\Omega^2[\beta - \tfrac{1}{2}(1+\alpha)]\} \\ -\Omega^2 & -(1+\alpha)\Omega^2 & \alpha\beta(K/K^a)\Omega^2 + \Omega^2[\beta - \tfrac{1}{2}(1+\alpha)] \end{bmatrix} \tag{26}$$

$$\mathbf{L} = \frac{\beta\Omega^2}{K^a D}\begin{Bmatrix} 1 \\ \gamma/\beta \\ 1/\beta \end{Bmatrix} \tag{27}$$

with $D = 1 + (1+\alpha)\beta(K/K^a)\Omega^2$, $\mathbf{x}_i = \{d_i, \Delta t v_i, \Delta t^2 a_i\}^T$, $\Omega = \omega^a \Delta t$ and $\omega^a = \sqrt{K^a/M}$ is the actual angular frequency of a structure. K^a represents the actual stiffness of a structure, which has to be lower than or equal to the predictor stiffness, K, to attain unconditional stability.[21] For free vibrations, equation (25) leads to the following analytical expression:[4]

$$d_n = \sum_{i=1}^{n} c_i \lambda_i^n = \exp(-\bar{\xi}\bar{\omega}\Delta t n)(c_1 \cos \bar{\omega}\Delta t n + c_2 \sin \bar{\omega}\Delta t n) + c_3 \lambda_3^n \tag{28}$$

in which λ_i represents the ith eigenvalue of **A**, $\bar{\xi}$ is the numerical damping ratio, $\bar{\omega}$ is the damped numerical frequency and the c_i's are constants determined from the initial conditions. In equation (28), λ_3 is a spurious root which is negligible when compared to $\lambda_{1,2}$.[22] If one represents $\lambda_{1,2} = B \pm iC$, then $\bar{\xi} = -\ln(B^2 + C^2)/2\bar{\Omega}$ and $\bar{\Omega} = \arctan(C/B)$, where $\bar{\Omega} = \bar{\omega}\Delta t$. In addition, one can express the spectral radius of matrix **A** as $\rho = \sqrt{B^2 + C^2}$. When $\alpha \neq 0$, lengthy expressions are available for variables B and C and, therefore, only a graphical representations is given for the quantities defined above. For the case of $\alpha = -1/3$, the spectral radius ρ is plotted against Ω in Figure 3(a), the numerical damping ratio $\bar{\xi}$ is represented in Figure 3(b), and the frequency error $(\Omega - \bar{\Omega})/\Omega$ is shown in Figure 3(c). One can observe in Figure 3(b) that the dissipation effect is small when the K^a/K ratio is small, i.e. when the predictor stiffness K is much larger than the actual stiffness K^a. On the other hand, as shown in Figure 3(c), the frequency distortion increases as the K^a/K ratio decreases.

When $\alpha = 0$ ($\gamma = \frac{1}{2}$ and $\beta = \frac{1}{4}$), the α–OSM algorithm becomes the OSM algorithm.[2] In this case, $\lambda_3 = 0$ and coefficients B and C lead to the following relations:

$$\rho = 0, \quad \bar{\xi} = 0, \quad \bar{\Omega} = \arctan \frac{\Omega\sqrt{4(1 + \frac{1}{4}(K/K^a)\Omega^2) - \Omega^2}}{2 + (1 + \frac{1}{4}(K/K^a)\Omega^2) - \Omega^2} \tag{29}$$

The frequency error $(\Omega - \bar{\Omega})/\Omega$ for the above case is plotted against Ω in Figure 4. It can be observed that when $\alpha = 0$, the frequency distortion is slightly reduced as compared to $\alpha = -1/3$.

When the predictor stiffness is equal to the actual stiffness, the α–C algorithm is identical to the constant-average-acceleration method. It has been shown by Dahlquist[23] that the constant-average-acceleration method provides the smallest frequency distortion among all the unconditionally stable second-order schemes. The frequency distortion for this case is shown in Figure 3(d). It can be observed that it is much smaller than that in the previous cases.

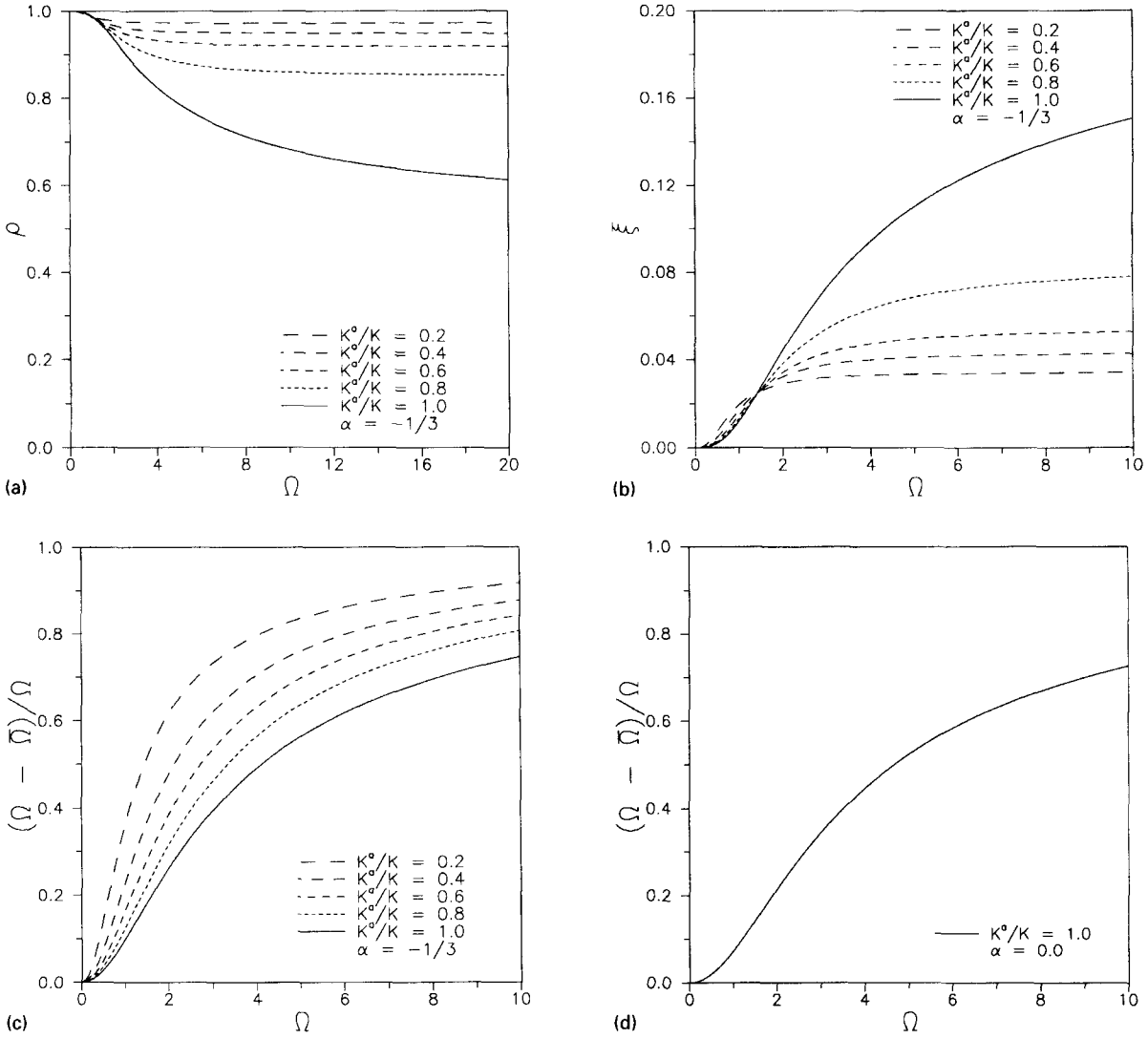

Figure 3. The α–OSM algorithm with $\alpha = -1/3$: (a) spectral radius; (b) algorithmic damping ratio; (c) frequency error; (d) the α–C algorithm with $\alpha = 0{\cdot}0$

COMPARISON OF IMPLICIT ALGORITHMS WITH EXPERIMENTAL ERRORS

In a pseudodynamic test, control and measurement errors are the most important indicators of the quality of a test, and their effects have been studied extensively.[10–16,18,19] Indeed, the error-correction method and the *I-Modification* adopted in the α–C and α–OSM algorithms, respectively, are intended to suppress the effects of these errors.

The analysis of the error effects in the α–C algorithm has already been performed by Shing *et al.*[3] With the same approach, the error effects of the α–OSM algorithm are analysed in the following sections. To distinguish the dissipation effects introduced by the α–OS algorithm and the *I-Modification*, two cases are considered here. In one case, only the α–OS algorithm is analysed. In the other case, the OSM algorithm, in which α is set equal to zero, is analysed. Finally, the performances of the implicit algorithms presented previously are compared by means of numerical simulations.

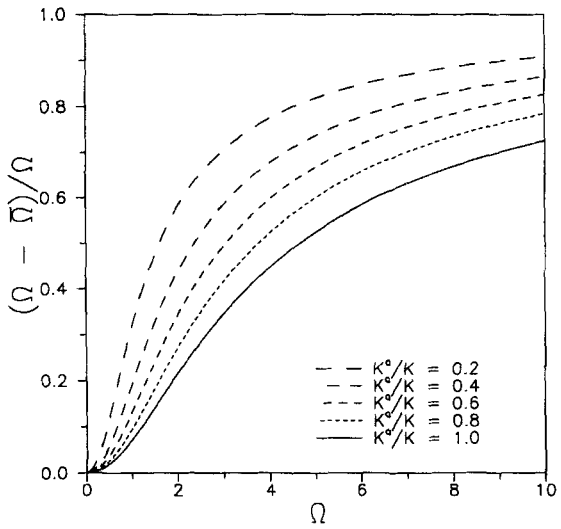

Figure 4. Frequency error in the OSM algorithm

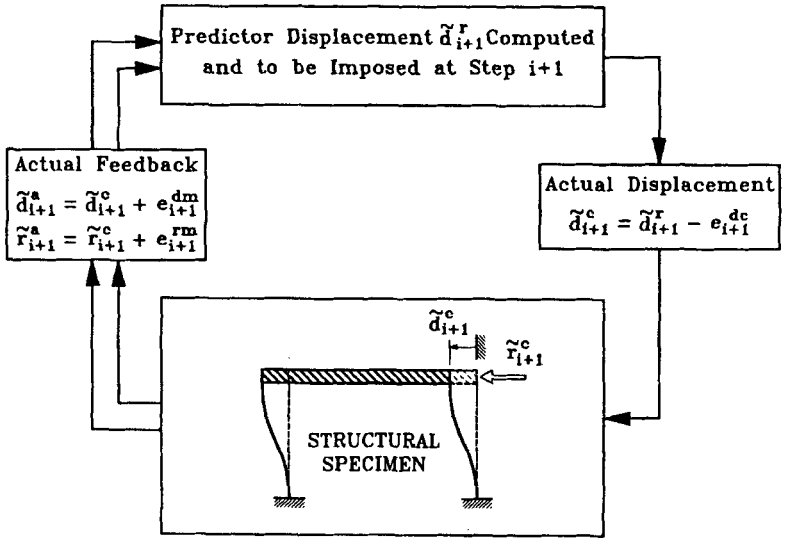

Figure 5. Schematic of the test method and sources of experimental errors

Experimental errors

The schematic of a pseudodynamic test method with typical sources of experimental errors is shown in Figure 5. These errors include the displacement control errors, e^{dc}_{i+1}, and the displacement and force measurement errors, e^{dm}_{i+1} and e^{rm}_{i+1}. These control and measurement errors amount to the total feedback errors introduced in each step of a test.[10] However, displacement and force measurement errors are usually substantially smaller than the displacement control errors e^{dc}_{i+1} and the corresponding force errors $K^{a}e^{dc}_{i+1}$. Thus, measurement errors are neglected from now on. As a result, the following relations hold:

$$\tilde{d}^{r}_{i+1} - \tilde{d}^{a}_{i+1} = e^{dc}_{i+1}, \quad \tilde{r}^{r}_{i+1} - \tilde{r}^{a}_{i+1} = K^{a}e^{dc}_{i+1} \tag{30}$$

in which $\tilde{d}^{r}_{i+1}$ and $\tilde{r}^{r}_{i+1}$ denote the exact numerical solutions evaluated from experimental feedback quantities, $\tilde{d}^{a}_{i+1}$ and $\tilde{r}^{a}_{i+1}$ are the actual values attained in the experiment, and K^{a} represents the actual stiffness of

a structure. In addition, $\tilde{d}_{i+1}$ and $\tilde{r}_{i+1}$ are used to represent the true numerical solutions in the absence of experimental errors.

Analysis of the α–OSM algorithm

The error-propagation analysis summarized here is based on the procedure developed by Shing and Mahin[10] for explicit time-stepping algorithms. With this approach, one considers an undamped linearly elastic single-degree-of-freedom system and defines the cumulative error vector $\bar{\varepsilon}_n$ as $(\mathbf{x}_n^r - \mathbf{x}_n)$, where $\mathbf{x}_n^r = \{d_n^r, \Delta t v_n^r, \Delta t^2 a_n^r\}^T$ denotes the exact numerical solution evaluated from experimental feedback quantities, and $\mathbf{x}_n$ the true numerical solution. By substituting $\mathbf{x}_n^r$ in equation (25) and using the relations in (30), one obtains the following expression:

$$\mathbf{x}_{i+1}^r = \mathbf{A}\mathbf{x}_i^r + (1+\alpha)\mathbf{L}(f_{i+1} + K^a e_{i+1}^{dc}) - \alpha\mathbf{L}(f_i + K^a e_i^{dc}) \tag{31}$$

Hence, subtracting equation (31) from equation (25) and performing repeated substitution with $\bar{\varepsilon}_0 = 0$, one obtains the cumulative errors induced by the stepwise control errors, e_i^{dc}:

$$\bar{\varepsilon}_n = \sum_{i=1}^{n} A^{n-i}\mathbf{L}g_{i+\infty} \tag{32}$$

For the α–algorithm, without the *I-Modification*,

$$g_{i+\alpha} = K^a e_{i+\alpha}^{dc} \tag{33}$$

where

$$e_{i+\alpha}^{dc} = e_i^{dc} + \alpha(e_i^{dc} - e_{i-1}^{dc}) \tag{34}$$

For the OSM algorithm, where one has to consider the correction of the restoring force as shown in equation (24) and set $\alpha = 0$,

$$g_i = -(K - K^a)e_i^{dc} = -(K - K^a)(\tilde{d}_i^r - \tilde{d}_i^a) \tag{35}$$

The value of g_i for the α–*C* algorithm with $\alpha = 0$ is given as

$$g_i = -(K - K^a)\Delta d_i \tag{36}$$

which is derived in Reference 3. In this case, Δd_i represents the residual displacement error after convergence is attained at step i.

To shed some light on the physical effect of these errors, the time history of d_i in a simple harmonic response and those of g_i given in equations (36), (33) and (35) are sketched in Figure 6, with the assumption that the errors Δd_i and e_i^{dc} are of the undershooting type. It should be mentioned that g_i is equivalent to an excitation force.[3] Hence, with the specific phase relations shown in Figure 6, g_i has a positive damping effect in the α–*C* algorithm,[3] a negative damping effect in the α–OS algorithm and a positive damping effect in the OSM algorithm. These damping effects are reversed if the errors e_i^{dc} are of the overshooting type.

By means of spectral decomposition of **A**, one can obtain from equation (32) the following relation:

$$\bar{e}_n^d = \sum_{i=1}^{n-1} \exp[-\bar{\xi}\bar{\omega}\Delta t(n-i-1)]e_i^{dc}\{c_1 \cos[\bar{\omega}\Delta t(n-i-1)] + c_2 \sin[\bar{\omega}\Delta t(n-i-1)]\} + \frac{\beta\Omega^2}{K^a D} g_n \tag{37}$$

The coefficients c_1 and c_2 are determined from equation (32) based on initial conditions. By introducing an amplification factor $D = \sqrt{c_1^2 + c_2^2}$ and ignoring the last term on the right-hand side of equation (37), one obtains

$$\bar{e}_n^d = D\sum_{i=1}^{n-1} \exp[-\bar{\xi}\bar{\omega}\Delta t(n-i)]e_i^{dc} \sin[\bar{\omega}\Delta t(n-i)] \tag{38}$$

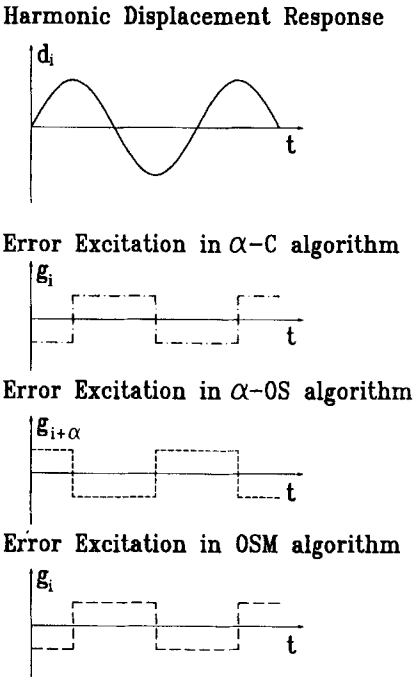

Figure 6. Time variation of error excitation for various algorithms

When $\alpha \neq 0$, lengthy expressions are associated with constants c_1 and c_2 and, therefore, only a graphical representation is given for the amplification factor D. However, these coefficients can be expressed in a compact form when $\alpha = 0$. For the OSM algorithm,

$$D = \frac{(K/K^a - 1)\Omega\sqrt{1 + \frac{1}{4}(K/K^a)\Omega^2 - \frac{1}{4}\Omega^2}}{(1 + \frac{1}{4}(K/K^a)\Omega^2)} \tag{39}$$

For the α–C algorithm[3] with $\alpha = 0$, it has been shown that

$$D = \frac{4\Omega}{4 + \Omega^2}\left(\frac{K}{K^a} - 1\right) \tag{40}$$

In the above case, e_i^{dc} in equation (38) should be replaced by Δd_i, which can be assumed to have the same order of magnitude as e_i^{dc}.

Factors D are plotted in Figures 7–9 for all three cases. The factor D expressed by equation (40) is plotted against Ω in Figure 7. Because $\lim_{\Omega \to \infty} D = 0$ for any finite value of the K^a/K ratio, the error effect diminishes in the α–C algorithm as the frequency increases. This is a highly desirable feature as spurious higher-mode responses are usually most disruptive. The same factor is represented in Figure 8 for the α–OS algorithm, with $\alpha = -1/3$. In this case, D does not exhibit a desirable behaviour for high frequencies in that it does not diminish as the frequency increases. However, for the α–OS algorithm, it should be noted that the algorithmic damping, i.e. the factor $\exp[-\bar{\xi}\bar{\omega}\Delta t(n - i)]$ in equation (38), contributes to the reduction of experimental error effects as well. Finally, the factor D expressed by equation (39) is plotted against Ω in Figure 9. In this case, $\lim_{\Omega \to \infty} D = 2(1 - K^a/K)\sqrt{(K/K^a - 1)}$. As a result, D is equal to zero only when the K^a/K ratio is equal to one.

Numerical examples

The error-propagation characteristics of the aforementioned algorithms are compared by means of numerical simulations in this section. The model considered here are an elastic two-storey shear

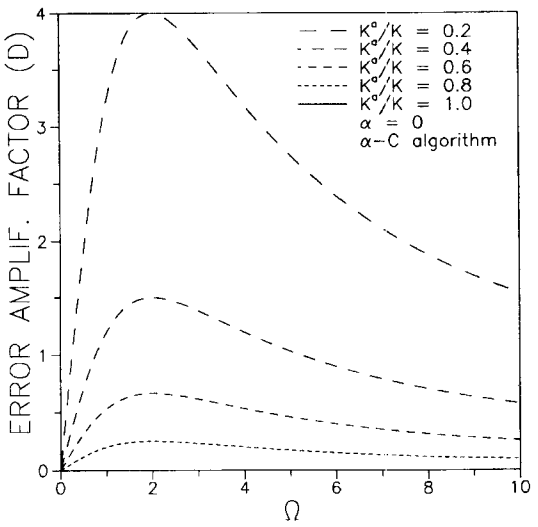

Figure 7. The error amplification factor for the α–C algorithm

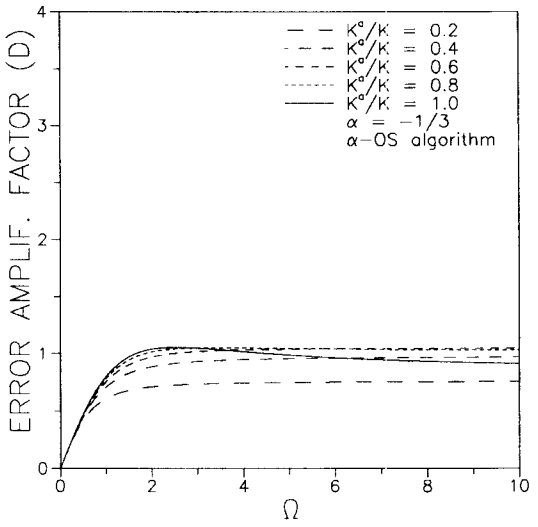

Figure 8. The error amplification factor for the α–OS algorithm

frame and a four-storey shear frame. Viscous damping is assumed to be zero, which is considered to be a stringent test.

All frames are subjected to the NS component of the 1940 El Centro ground motion, with its peak acceleration scaled to $0{\cdot}045g$ for the linear case. For the frame with strain hardening behaviour, a peak acceleration of $0{\cdot}18g$ is adopted.

Systematic undershooting errors which give rise to large cumulative errors in the structural response[10] are considered in these simulations. They are simply generated by introducing a constant undershoot in each step. For the purpose of comparison, the convergence tolerance Δd^n adopted in the α–C algorithm is equal to the magnitude of undershooting errors e^{dc}_{i+1}. However, such a comparison is only approximate in these simulations, because the convergence criterion expressed by the relation $|\Delta d_i| \leqslant \Delta d^n$ may engender a residual displacement Δd_i smaller than the tolerance.

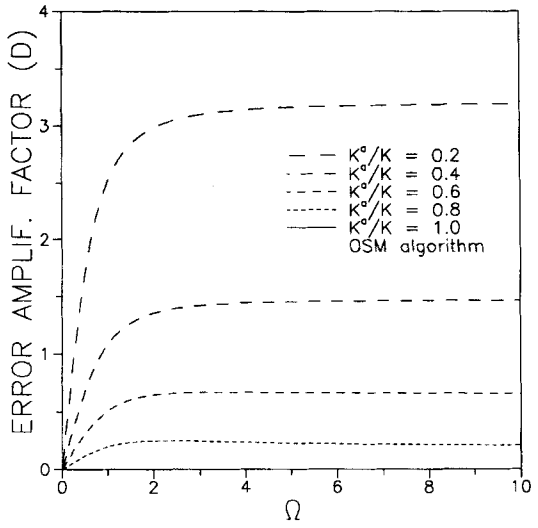

Figure 9. The error amplification factor for the OSM algorithm

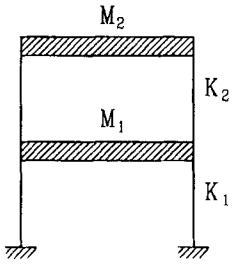

Figure 10. Two-storey shear frame

Table I. Properties of the elastic shear frame

Storey	Model properties		Modal frequencies	
i	M_i (kg)	K_i (kN/mm)	ω_1 (rad/s)	ω_2 (rad/s)
1	1751	1·4	11·2	35·7
2	3502	0·7		

Exact numerical solutions without any error are referred to as 'Exact' here. 'Exact' non-linear solutions are obtained with the constant-average-acceleration method, by using a small displacement tolerance of $\Delta d^n = 2{\cdot}54 \times 10^{-5}$ mm for each degree of freedom.

Linearly elastic two-degree-of-freedom system

The model problem considered here is the elastic two-storey shear frame illustrated in Figure 10. The properties and frequencies of the structure are collected in Table I. An integration time interval of 0·035 s, which is about $\frac{1}{16}$ of the fundamental period of the frame, is selected for all simulations. The stiffness factor, SF, which is defined as $\mathbf{K} = (1/\mathrm{SF}) \cdot \mathbf{K}^a$, is assumed to be 0·8. In all simulations, constant undershooting errors of 0·183 mm are considered.

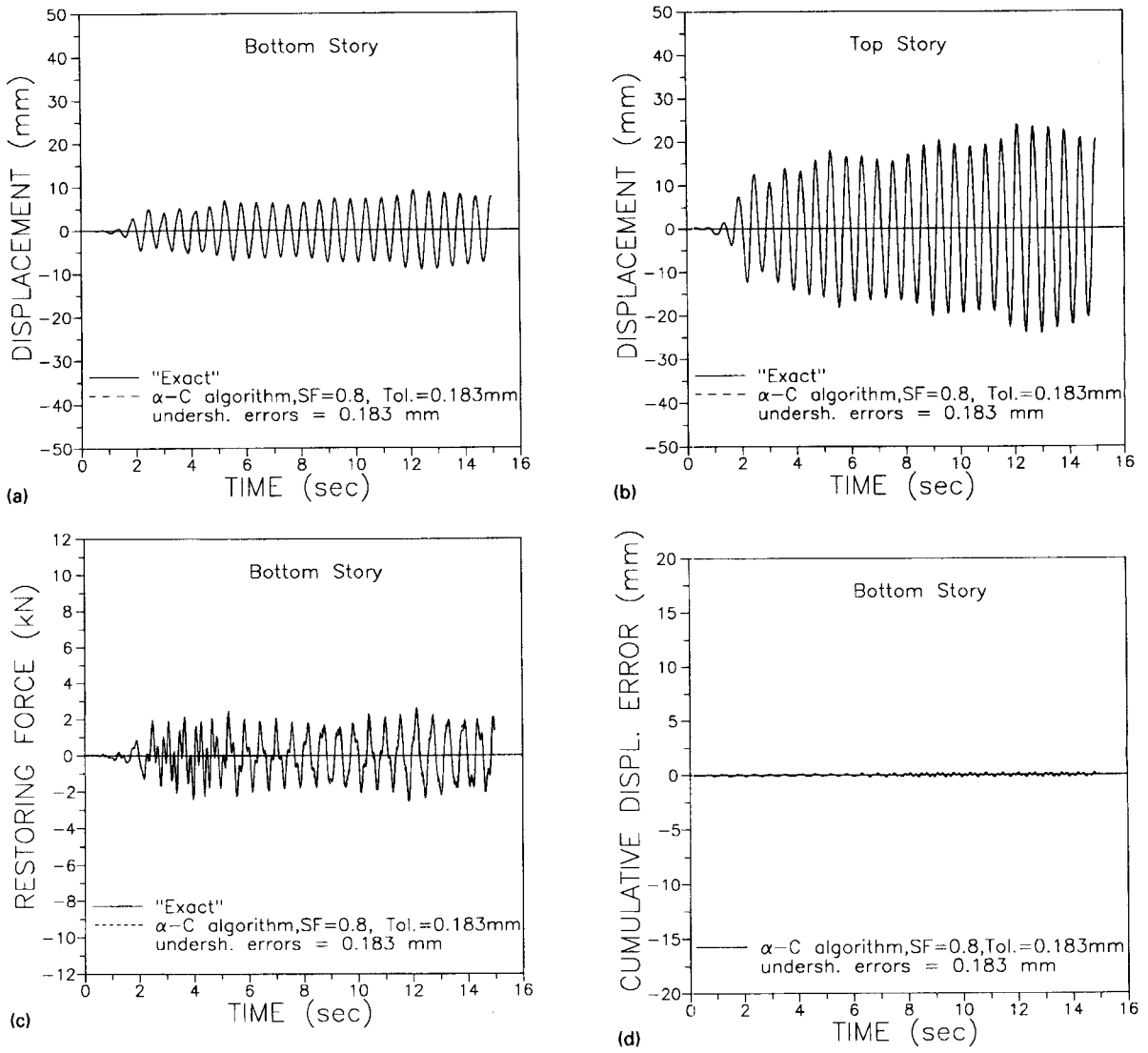

Figure 11. Response of a two-storey frame to the 1940 El Centro ground motion with the α–C algorithm, $\alpha = 0$ and undershooting errors of 0·183 mm: (a)–(b) displacement time histories; (c) restoring force time history; (d) cumulative displacement error time history

The displacement time histories of both storeys obtained with the α–C algorithm, where $\alpha = 0$, are shown in Figures 11(a)–11(b), while the restoring force time history of the bottom storey is shown in Figure 11(c). The good performance of the algorithm is evident. This trend is also confirmed by observing the cumulative displacement error at the bottom storey, which is shown in Figure 11(d).

The displacement time histories obtained with the α–OS algorithm are shown in Figures 12(a)–12(b), while the restoring force time history and the growth of the cumulative displacement error at the bottom storey are illustrated in Figures 12(c) and 12(d), respectively. It can be observed that the second-mode response is excited by the undershoot errors [see Figure 12(c)], as expected from the previous discussions (Figure 6). One can observe that even with a value of α approaching the limit of $-\frac{1}{3}$, the cumulative errors cannot be controlled effectively. Based on these results, one can conclude that α-damping does not represent an effective way to control cumulative errors when the feedback errors are large.

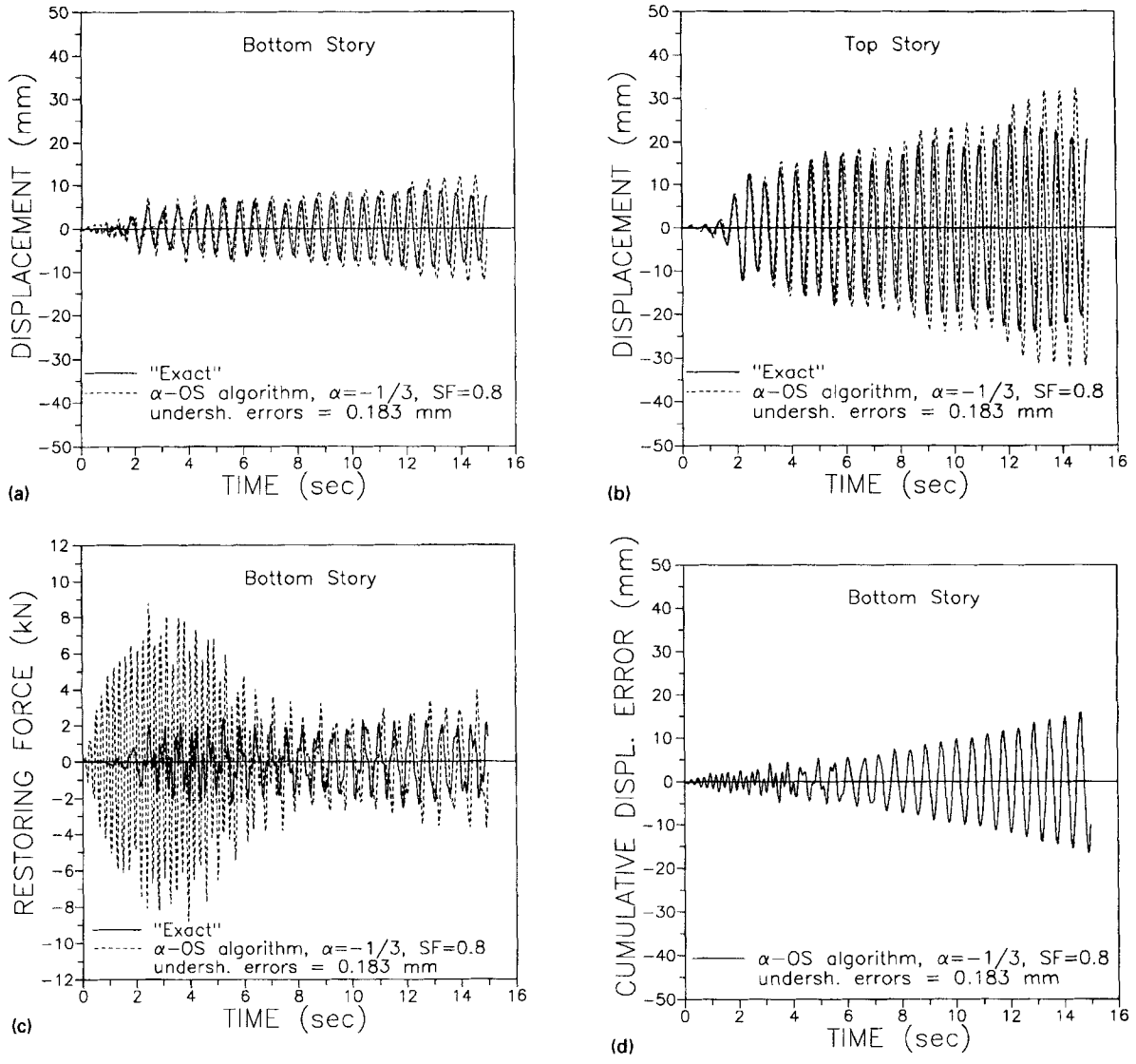

Figure 12. Response of a two-storey frame to the 1940 El Centro ground motion with the α–OS algorithm, α = -- 1/3 and undershooting errors of 0·183 mm: (a)–(b) displacement time histories; (c) restoring force time history; (d) cumulative displacement error time history

The corresponding displacement time histories determined with the OSM algorithm are shown in Figures 13(a) and 13(b). It can be observed that the *I-Modification* can suppress effectively the error growth by introducing a positive damping effect. The restoring force time history developed at the bottom storey is shown in Figure 13(c). Finally, the cumulative displacement error associated with the bottom storey is plotted in Figure 13(d). It is larger than the cumulative displacement error associated with the α–*C* algorithm [see Figure 11(d)] due to the higher-frequency distortion effects introduced by the OSM algorithm.

Inelastic four-degree-of-freedom system

The inelastic shear frame shown in Figure 14(a) is analysed here by assuming a stiffness factor, SF, equal to 0·87, which is defined with respect to the initial stiffness of the structure. As previously shown, the α-damping

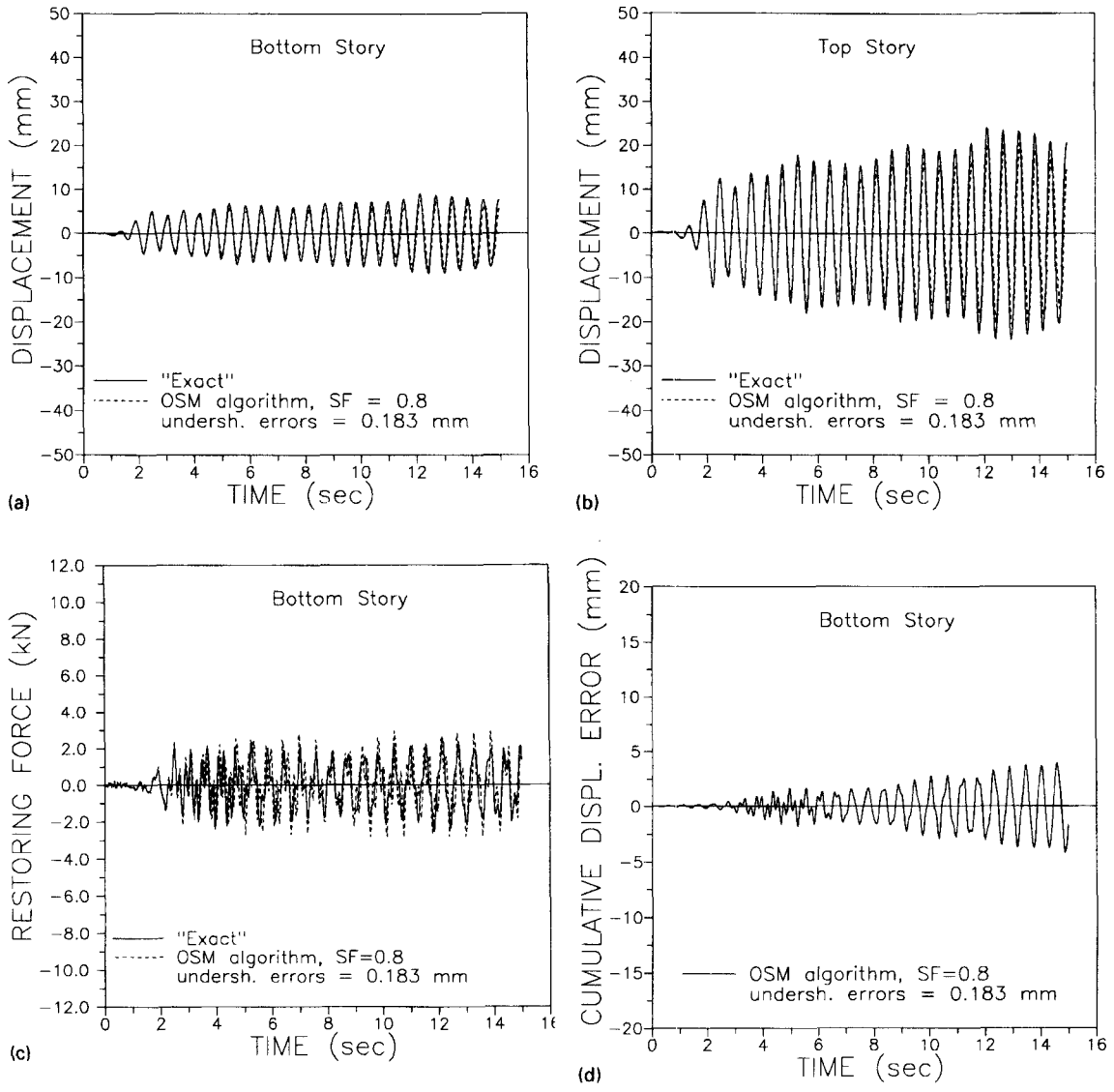

Figure 13. Response of a two-storey frame to the 1940 El Centro ground motion with the OSM algorithm and undershooting errors of 0·183 mm: (a)–(b) displacement time histories; (c) restoring force time history; (d) cumulative displacement error time history

cannot control effectively the experimental errors. Therefore, only the α–C algorithm with $\alpha = 0$ and the OSM algorithm are considered in these simulations.

The non-linearity at each storey of the strain hardening frame is modelled with the Giuffrè–Menegotto–Pinto model shown in Figure 14(b). The properties of the frame model and the values of the stiffness and strength parameters defining the constitutive relation of each storey are collected in Table II. The modal frequencies are also shown in the same table. An integration time interval equal to 0·035 s, which is about $\frac{1}{23}$ of the fundamental period of the frame, is selected for these simulations. In addition, an undershooting error of 0·5 mm is considered.

The responses obtained with the α–C algorithm with $\alpha = 0$, in terms of displacement and restoring force histories, are compared to the 'Exact' numerical responses in Figures 15(a)–15(d). One can observe the good performance of this algorithm in the non-linear regime. The corresponding responses determined with the

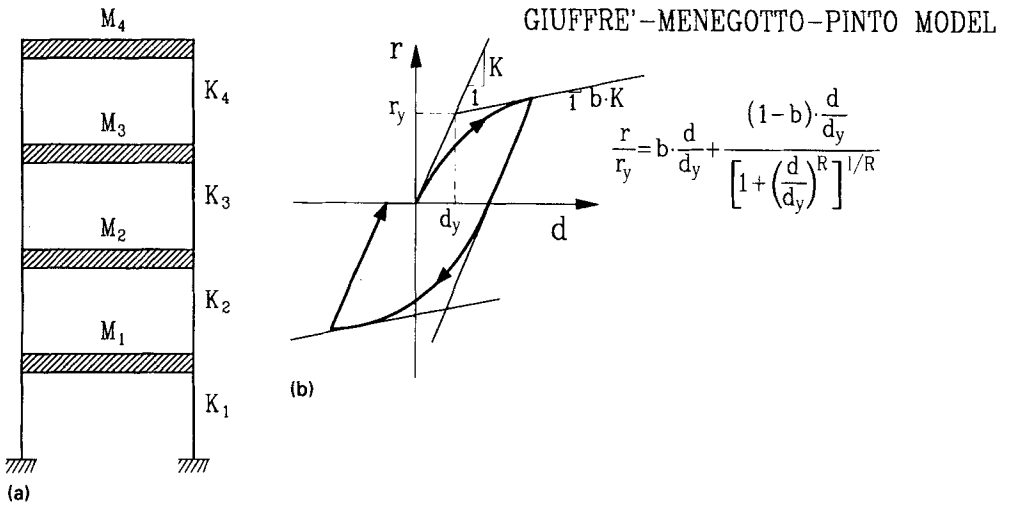

Figure 14. (a) Four-storey shear frame; (b) the inelastic constitutive model

Table II. Properties of the strain hardening shear frame

Storey	Model properties						Modal frenquencies			
i	M_i (kg)	K_i (kN/mm)	d_y (mm)	r_y (kN)	b	R	ω_1 (rad/s)	ω_2 (rad/s)	ω_3 (rad/s)	ω_4 (rad/s)
1	1751	1·4	6·35	8·9	0·02	4·0	7·7	21·2	37·9	51·5
2	1751	1·4	6·35	8·9	0·02	4·0				
3	1751	1·4	6·35	8·9	0·02	4·0				
4	3502	0·7	12·7	8·9	0·02	4·0				

OSM algorithm are shown in Figure 16. In this case, the algorithm can capture the main characteristics of the response. However, inaccuracies in displacement time histories can be observed in Figures 16(a) and 16(b). These algorithms have exhibited similar performances for structures that have a strain softening-type non-linearity.[24]

VERIFICATION TESTS

The steel beam shown in Figure 17(a) has been designed to substantiate the theoretical findings presented above. The specimen selected is modelled as a two-degree-of-freedom cantilever structure, which is shown in Figure 17(b). The elastic stiffness matrix $\mathbf{K}^m$ measured from the specimen is shown in the same figure. The translational masses are selected to be 17 512 and 35 024 kg for degree-of-freedom one (DOF 1) and two (DOF 2), respectively. The resulting natural frequencies are 4·6 and 24·2 rad/s. Free-vibration pseudodynamic tests have indicated that the set-up has an energy-dissipation property equivalent to 1 per cent viscous damping in the first mode, and 0·64 per cent in the second mode due to friction in the system. In the tests, a null damping matrix has been adopted.

For all tests, the NS component of the 1940 El Centro ground motion has been scaled to have a 0·0072g peak acceleration. Hence, the structural response should remain elastic under these conditions. The predictor stiffness $\mathbf{K}$ is chosen to be the measured stiffness $\mathbf{K}^m$ divided by a stiffness factor, SF, of 0·75 to assure that $\delta\mathbf{K} = \mathbf{K} - \mathbf{K}^a$ is always positive semi-definite.

A digital controller has been used for test control and data acquisition. Both actuators are calibrated to a displacement range of ± 152 mm. The D/A and A/D converters in the interface have a 16-bit resolution

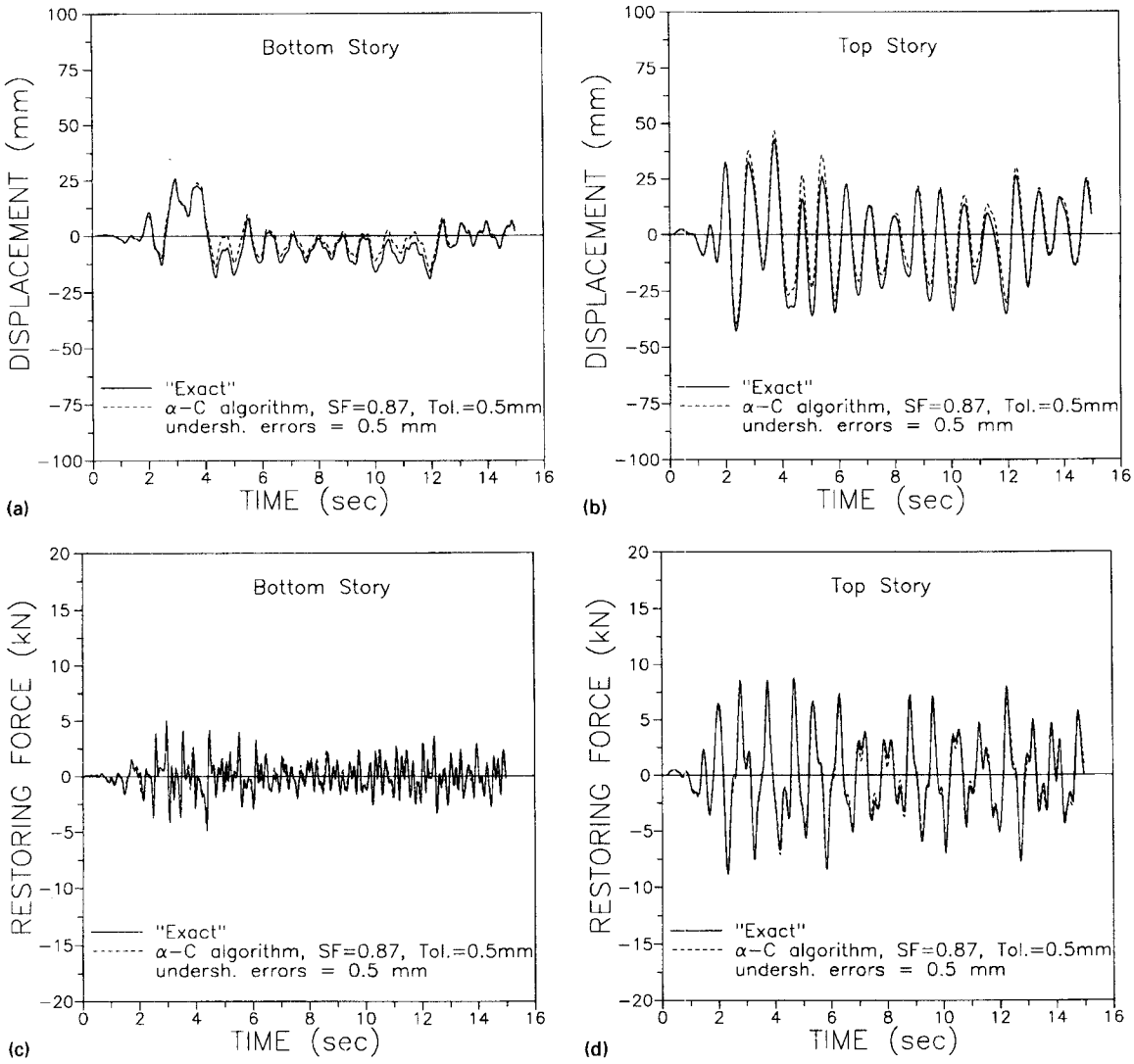

Figure 15. Response of a four-storey frame to the 1940 El Centro ground motion with the α–C algorithm, $\alpha = 0$ and undershooting errors of 0·508 mm: (a)–(b) displacement time histories; (c)–(d) restoring force time histories

and, therefore, the resolution of displacement control and feedback signals is $4{\cdot}6 \times 10^{-3}$ mm. A tolerance of $\Delta d^n = 2{\cdot}54 \times 10^{-2}$ mm is used for both degrees of freedom in the α–C algorithm. This tolerance corresponds to about 2 per cent of the maximum displacement expected at DOF 2.

Both the α–C and OSM algorithms have been implemented with a dual displacement control by adopting displacement transducers external as well as internal to hydraulic actuators. The dual displacement control in the OSM algorithm is carried out by controlling the actuator displacements with internal LVDTs and performing the *I-Modification* with readings from the external LVDTs. The OSM algorithm has also been implemented with displacement control through external LVDTs.[25] In all simulations, $\alpha = 0$ for the α–C algorithm.

The first set of experiments has been performed by using an integration time interval equal to 0·02 s, which is small when compared to the fundamental period of the specimen. The responses obtained with the α–C algorithm are compared with the 'Exact' numerical responses in Figure 18. One can observe the good

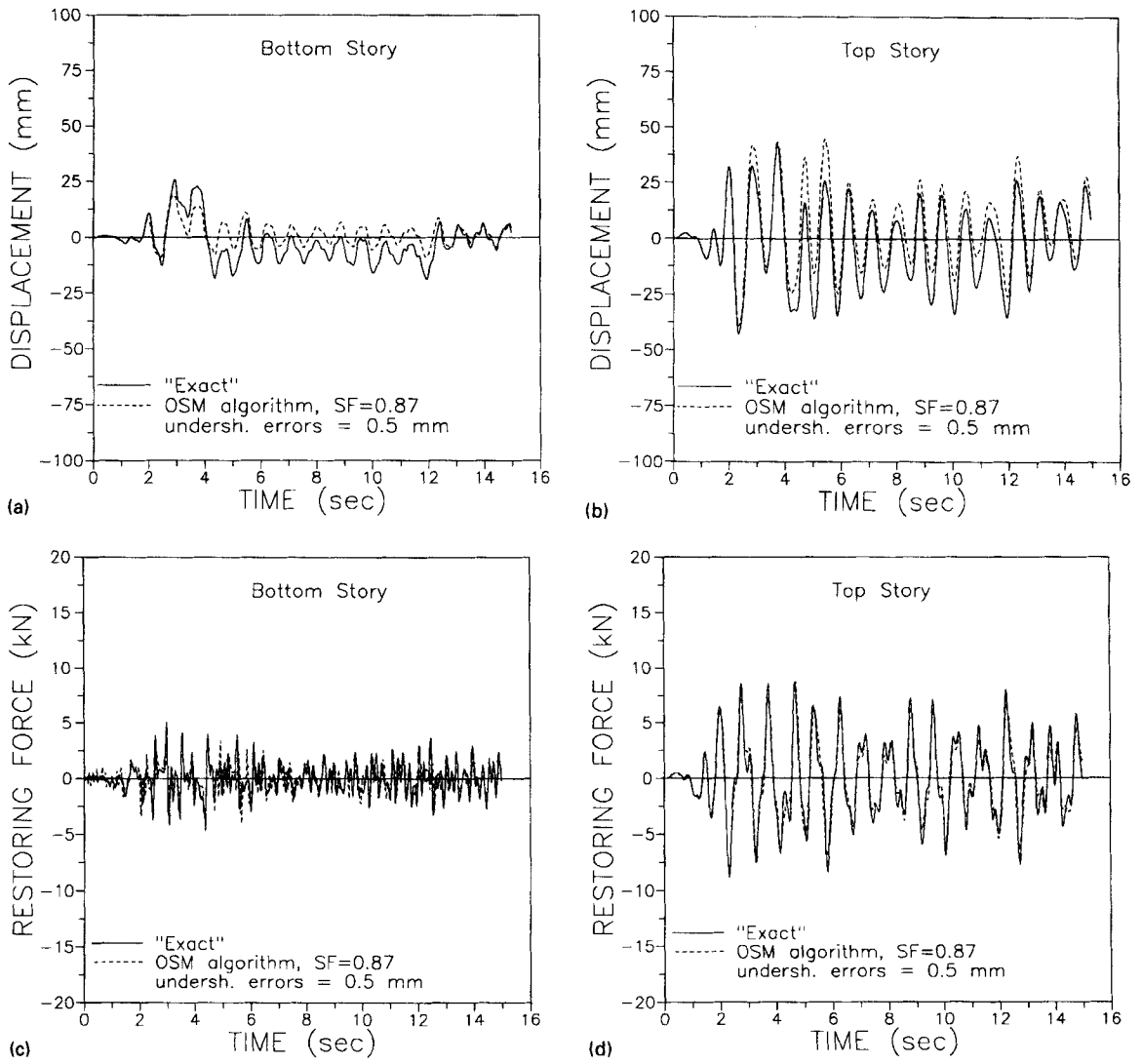

Figure 16. Response of a four-storey frame to the 1940 El Centro ground motion with the OSM algorithm and undershooting errors of 0·508 mm: (a)–(b) displacement time histories; (c)–(d) restoring force time histories

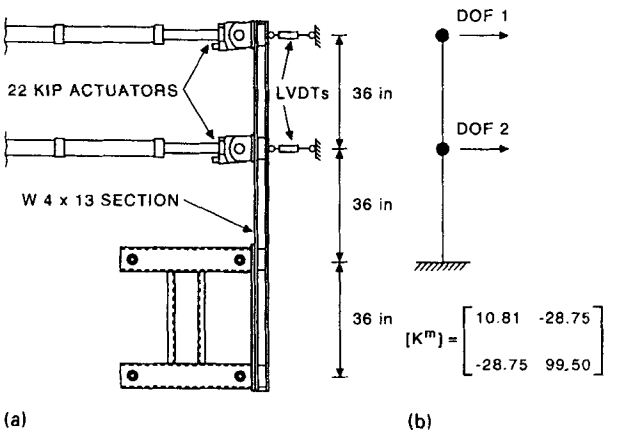

Figure 17. Test specimen. (a) test set-up; (b) analytical model (1 in = 0·0254 m; 1 kip/in = 175·2 kN/m)

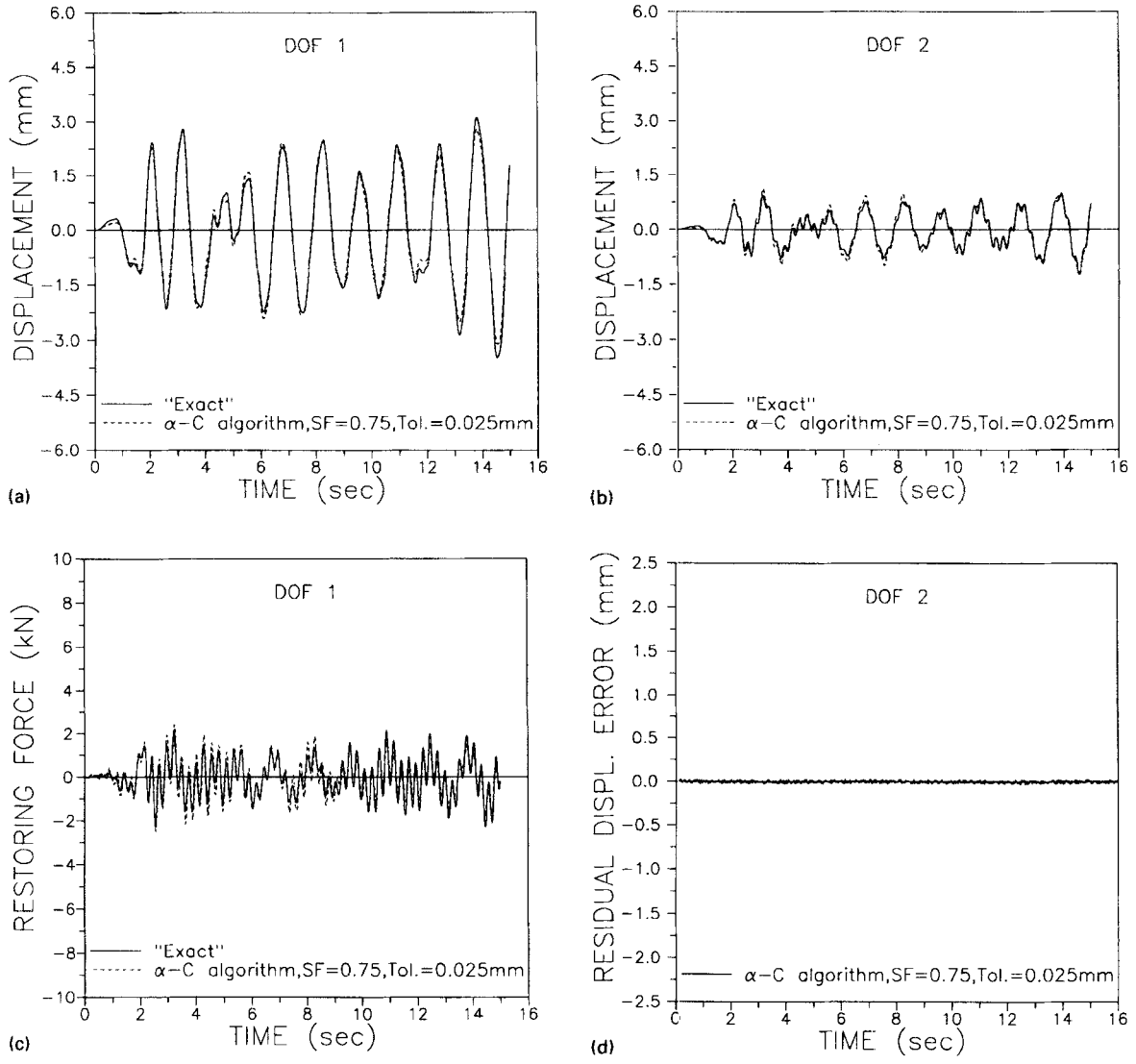

Figure 18. 2-DOF experimental responses to the 1940 El Centro ground motion with the α–C algorithm, $\alpha = 0$, $\Delta t = 0{\cdot}02$ s and dual displacement control: (a)–(b) displacement time histories; (c) restoring force time history; (d) residual displacement error time history

performance of the α–C algorithm. Figure 18(d) shows the time history of the residual displacement errors at DOF 2.

The corresponding responses determined with the OSM algorithm are shown in Figures 19(a)–19(c), together with the 'Exact' displacement and restoring force time histories. The algorithm also demonstrates excellent performance. The displacement errors at DOF 2, defined as the difference between the target displacement and the displacement measured with the external LVDTs, are shown in Figure 19(d).

The second set of experiments have been conducted by using an integration time interval of 0·06 s, which is about $\frac{1}{24}$ of the fundamental period of the specimen. The results obtained with the α–C algorithm are compared with the 'Exact' numerical simulations in Figure 20. In this test, the experimental results are as accurate as those obtained in the previous test.

The response time histories determined with the OSM algorithm are plotted in Figure 21, with the 'Exact' simulated responses. It can be observed from Figures 21(a) and 21(b) that the displacement time histories are

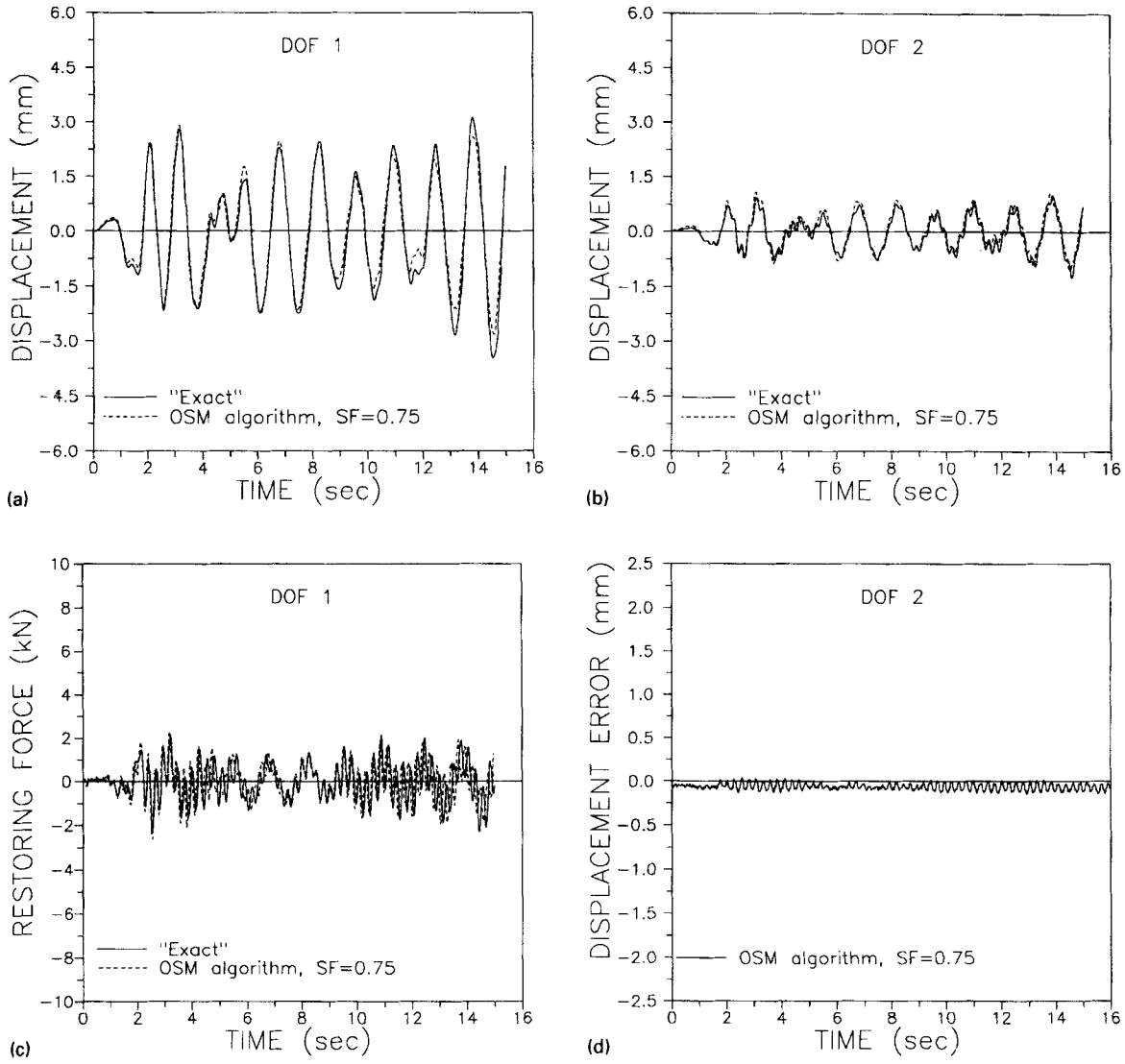

Figure 19. 2-DOF experimental responses to the 1940 El Centro ground motion with the OSM algorithm, $\Delta t = 0{\cdot}02$ s and dual displacement control: (a)–(b) displacement time histories; (c) restoring force time history; (d) displacement error time history

quite accurate. However, the restoring force time history, which is illustrated in Figure 21(c), exhibits a significant error. This is probably due to the larger displacement errors shown in Figure 21(d) as compared to those shown in Figure 19(d). One disadvantage of the OSM scheme presented here is that there is no control on displacement errors which rely totally on the performance of the actuators. While the implementation of an explicit control on displacement errors is possible with the OSM method,[25] it necessitates an iteration correction which reduces the attractiveness of the non-iterative method. It should be mentioned that the experimental results show a similar trend when external LVDTs are used for displacement control with the OSM algorithm.

In general, one should notice from Figure 18(d)–21(d) that the displacement errors introduced in the tests conducted with the OSM algorithm are a lot higher than those with the α–C algorithm due to the aforementioned fact.

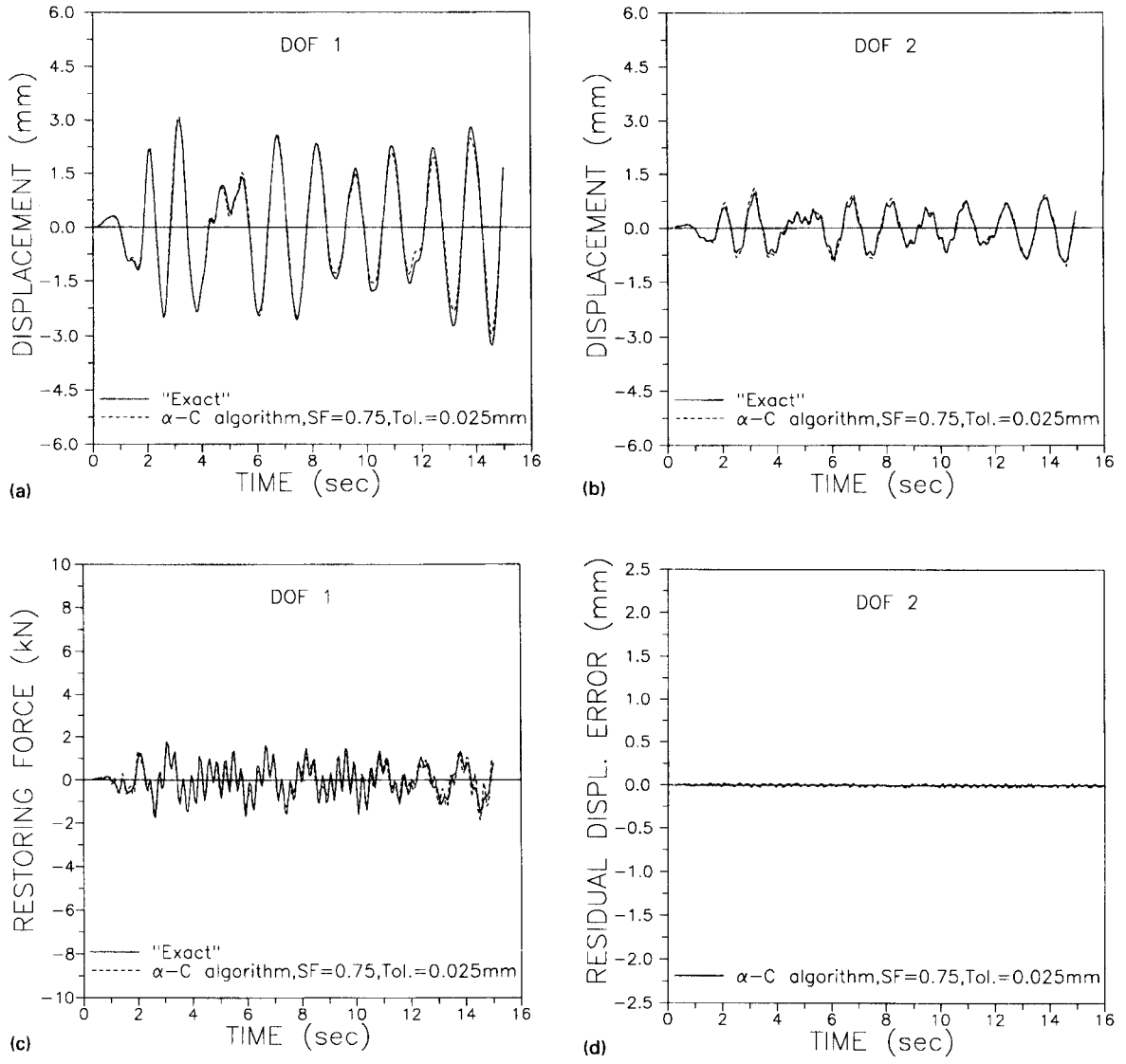

Figure 20. 2-DOF experimental responses to the 1940 El Centro ground motion with the α–C algorithm, $\alpha = 0$, $\Delta t = 0{\cdot}06$ s and dual displacement control: (a)–(b) displacement time histories; (c) restoring force time history; (d) residual displacement error time history

CONCLUSIONS

Implicit time-stepping algorithms which have been used for pseudodynamic tests have been summarized in this paper. In particular, the α–C and α–OSM algorithms have been investigated in a consistent manner through theoretical analysis, numerical simulations and verification tests. It has been shown that the α–C algorithm can control the experimental error effects effectively. For the α–OS algorithm, it has been demonstrated that undershooting errors introduce energy adding effects which cannot be suppressed effectively with algorithmic damping. In the case of the α–OSM algorithm, the *I-Modification* represents an effective means to mitigate the effects of experimental errors because it introduces an energy-dissipation effect when errors are of the undershooting type.

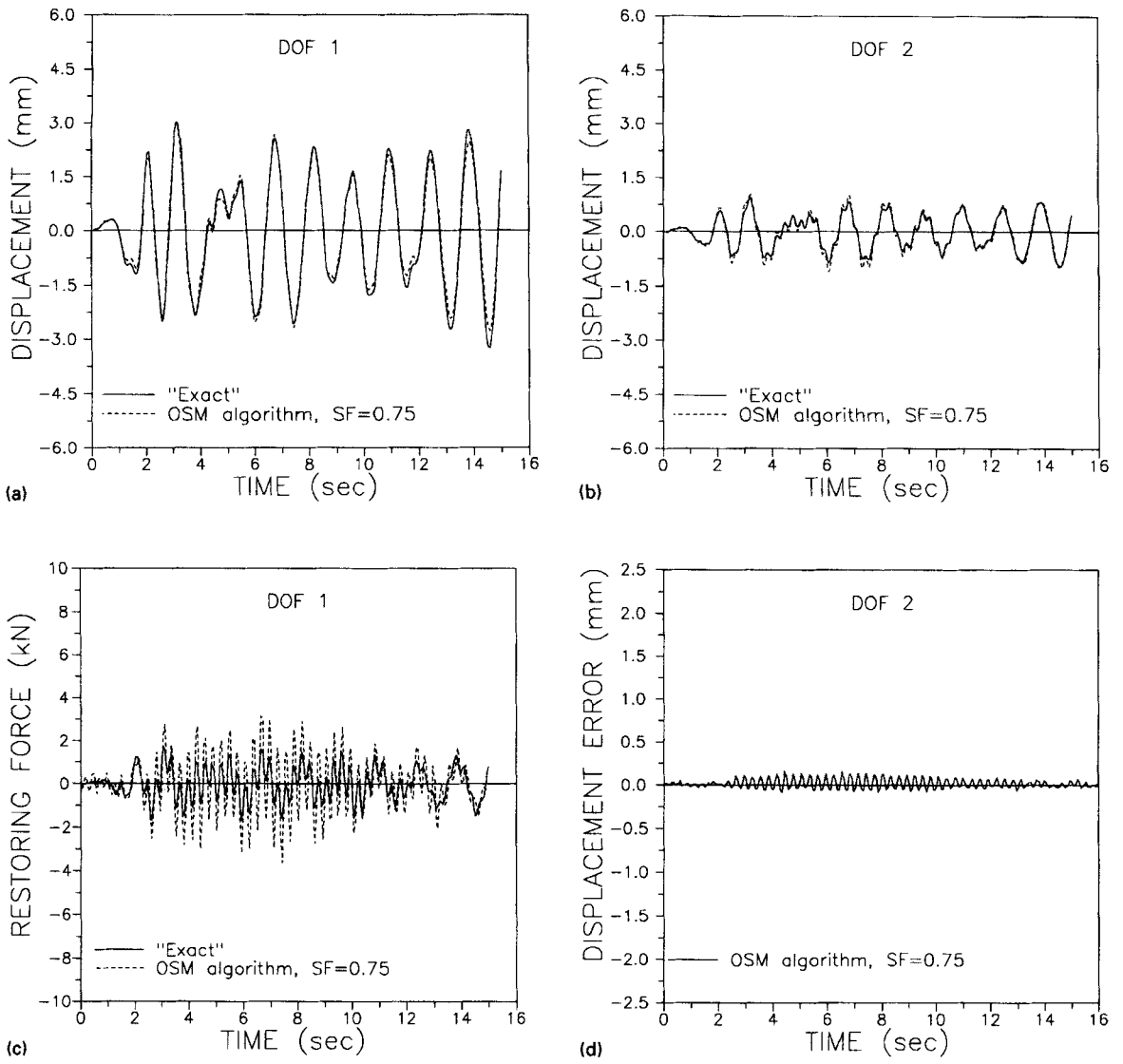

Figure 21. 2-DOF experimental responses to the 1940 El Centro ground motion with the OSM algorithm, $\Delta t = 0{\cdot}06$ s and dual displacement control: (a)–(b) displacement time histories; (c) restoring force time history; (d) displacement error time history

ACKNOWLEDGEMENTS

The study conducted here was sponsored by MURST, CNR of Italy under Grant No. 93.02186.CT07 and MTS Systems Corporation. However, opinions expressed in this paper are those of the writers, and do not necessarily reflect those of the sponsors. The authors are also grateful to Zorica Radakovic-Guzina for her assistance in the experimental work.

REFERENCES

1. C. R. Thewalt and S. A. Mahin, 'Hybrid solution techniques for generalized pseudodynamic testing', *Report No. UCB/EERC-87/09*, Earthquake Engineering Research Center, University of California Berkeley, CA, 1987.
2. M. Nakashima, T. Kaminosono, M. Ishida and K. Ando, 'Integration techniques for substructure pseudodynamic test', *Proc. 4th U.S. natl conf. earthquake eng.*, Palm Springs, CA, Vol. II, 1990, pp. 515–524.

3. P. B. Shing, M. T. Vannan and E. Carter, 'Implicit time integration for pseudodynamic tests', *Earthquake eng. struct. dyn.* **20**, 551–576 (1991).
4. H. M. Hilber, T. J. R. Hughes and R. L. Taylor, 'Improved numerical dissipation for time integration algorithms in structural dynamics', *Earthquake eng. struct. dyn.* **20**, 283–292 (1977).
5. T. J. R. Hughes, K. S. Pister and R. L. Taylor, 'Implicit–explicit finite elements in non-linear transient analysis', *Comput. methods appl. mech. eng.* **17/18**, 159–182 (1979).
6. K.-C. Tsai, J.-W. Li and T.-F. Wang, 'Pseudodynamic performance of steel plate energy-dissipating substructures', *Proc. 5th U.S. natl conf. earthquake eng.*, Chicago, IL, Vol. I, 1994, pp. 735–744.
7. O. S. Bursi, P. B. Shing and Z. Radakovic-Guzina, 'Pseudodynamic testing of strain-softening systems with adaptive time steps', *Earthquake eng. struct. dyn.* **23**, 745–760 (1994).
8. F. Seible, G. A. Hegemier, A. Igarashi and G. R. Kingsley, 'Simulated seismic-load tests on full-scale five-story masonry building', *J. struct. eng. ASCE* **120**, 903–924 (1994).
9. P. B. Shing, O. S. Bursi and M. T. Vannan, 'Pseudodynamic tests of a concentrically braced frame using substructuring techniques', *J. constr. steel res.* **29**, 121–148 (1994).
10. P. B. Shing and S. A. Mahin, 'Cumulative experimental errors in pseudodynamic tests', *Earthquake eng. struct. dyn.* **15**, 409–424 (1987).
11. M. Nakashima and H. Kato, 'Experimental error growth behavior and error growth control in on-line computer test control method', *Research Paper 123*, Building Research Institute, Ministry of Construction, Japan, 1987.
12. R. Peek and W.-H. Yi, 'Error analysis for the pseudodynamic test method, I: analysis', *J. eng. mech. ASCE* **116**, 1618–1637 (1990).
13. R. Peek and W.-H. Yi, 'Error analysis for the pseudodynamic test method. II: application', *J. eng. mech. ASCE* **116**, 1638–1658 (1990).
14. P. B. Shing and M. T. Vannan, 'On the accuracy of an implicit algorithm for pseudodynamic tests', *Earthquake eng. struct. dyn.* **19**, 631–651 (1990).
15. D. Comberscure and P. Pegon, 'Alpha-operator splitting time integration technique for pseudodynamic testing: error propagation analysis', *Special Publication, No. I.94.65, CEC, JRC*, Ispra, Italy, 1994.
16. M. Nakashima, T. Akazawa and O. Sakaguchi, 'Integration method capable of controlling experimental error growth in substructure pseudo dynamic test', *J. struct. constr. eng. AIJ* **454**, 61–71 (1993).
17. P. B. Shing, O. S. Bursi, Z. Radakovic-Guzina and M. T. Vannan, 'Recent developments in pseudodynamic testing based on an implicit time integration method', *U.S.–Japan Seminar on Developments and Future Dimensions of Structural Testing Techniques*, Hawaii, 28 June–1 July 1993.
18. W.-H. Yi and R. Peek, 'Posterior time-step adjustment in pseudodynamic testing', *J. eng. mech ASCE* **119**, 1376–1386 (1993).
19. C. Thewalt and M. Roman, 'Performance parameters for pseudodynamic tests', *J. struct. eng. ASCE* **120**, 2768–2781 (1994).
20. O. S. Bursi and P. B. Shing, 'Adaptive time steps and secant-Newton iterations for pseudodynamic testing of strain-softening structures', *Proc. 5th U.S. natl conf. earthquake eng.*, Chicago, IL, Vol. I, 1994, pp. 753–762.
21. M. E. Plesha and T. Belytschko, 'A constitutive operator splitting method for nonlinear transient analysis', *Comput. struct.* **20**, 767–777 (1990).
22. G. M. Hulbert and J. Chung, 'The unimportance of the spurious root of time integration algorithms for structural dynamics', *Commun. numer. methods eng.* **10**, 591–597 (1994).
23. G. Dahlquist, 'A special stability problem for linear multistep methods', *BIT* **3**, 27–43 (1963).
24. O. S. Bursi and P. B. Shing, 'Evaluation of implicit time-stepping algorithms for pseudodynamic tests', *Workshop on Cyclic Damage and Pseudodynamic tests*, Naples, Italy, 2–3 June 1994, pp. 159–198.
25. G. Magonette, 'Digital control of pseudodynamic tests', in J. Donea and P. M. Jones (eds), *Experimental and Numerical Methods in Earthquake Engineering*, Kluwer Academic Publishers, Dordrecht, 1991, pp. 63–99.